# Evanescent wave cavity ring-down spectroscopy for trace water detection

Andrew C. R. Pipino
and
Joseph T. Hodges

Process Measurements Division
National Institute of Standards and Technology
100 Bureau Drive
Gaithersburg, Maryland 20899-8363

## ABSTRACT

We explore the use of evanescent wave cavity ring-down spectroscopy (EW-CRDS) for water detection through a signal-to-noise ratio analysis. Cavity ring-down spectroscopy (CRDS) is an emerging optical absorption technique that employs the mean photon decay time of a high-finesse optical cavity as the absorption-sensitive observable. EW-CRDS is a novel implementation of CRDS that extends the technique to surfaces, films, and liquids by employing optical cavities which incorporate at least one total-internal-reflection (TIR) mirror. The concomitant evanescent wave is then used to probe the absorption of an ambient medium at the TIR surface also through a change in the photon decay time. By employing miniature monolithic cavities with ultra-smooth surfaces that are fabricated from ultra-high transmission materials, extreme sub-monolayer detection sensitivity is readily achieved. The detection of water by EW-CRDS with a fused-silica resonator provides an interesting and important application, since the nascent hydroxylated $SiO_2$ surface is expected to show a high natural affinity for adsorption of water through hydrogen-bonding interactions. Furthermore, in the 1380 nm spectral region where water absorbs strongly, low-OH-content fused silica has extremely high bulk transmission. These factors potentially provide the basis for a novel water sensor.

**Keywords:** cavity ring-down, evanescent waves, optical absorption, resonator design, water sensor, films.

## 1. INTRODUCTION

Cavity ring-down spectroscopy (CRDS) has been reviewed elsewhere.[1-4] The simplicity of operation of the technique combined with its potential for achieving near shot-noise-limited sensitivity at high fluence, make CRDS a very appealing diagnostic tool. CRDS utilizes the photon intensity decay time or "ring-down" time in a high-finesse (low-loss) optical cavity as the absorption-sensitive observable. In gas phase applications, the cavity typically consists of a pair of high reflectivity dielectric mirrors which are arranged to form a stable optical resonator. When light is injected into the cavity, the intensity decays exponentially with a ring-down time constant given by,

$$\tau(\omega)=\frac{t_r}{\mathcal{L}_0(\omega) + \mathcal{L}_{abs}(\omega)} \qquad (1)$$

where $\mathcal{L}_0(\omega)$ and $\mathcal{L}_{abs}(\omega)$ are the intrinsic and absorption loss, respectively, and $t_r$ is the round-trip time for light propagation in the cavity. By measuring the difference in the intensity decay rate, with and without an absorbing medium present, as a function of laser frequency, the absorption spectrum is obtained. Measurement of optical absorption is then achieved through a measurement of time. The minimum detectable absorption in CRDS or EW-CRDS can be expressed as the product of the intrinsic loss and the relative uncertainty in the ring-down time [5], or $(\mathcal{L}_{abs})_{min} = \mathcal{L}_0 * (\Delta\tau/\tau)_{min}$, which separates approximately into cavity- and instrumentation-dependent terms, respectively.

Advanced Environmental and Chemical Sensing Technology, Tuan Vo-Dinh, Stephanus Buettgenbach, Editors, Proceedings of SPIE Vol. 4205 (2001) © 2001 SPIE. · 0277-786X/00/$15.00

Optimization of sensitivity in CRDS is therefore achieved by minimizing the intrinsic cavity loss and measuring the ring-down time with the minimum uncertainty. CRDS has been employed mostly for gas phase diagnostics since a large intrinsic loss is introduced by most sampling schemes for liquids or films.

To extend CRDS to surfaces and condensed matter, evanescent wave CRDS (EW-CRDS) was developed[6-11], which employs total internal reflection (TIR) mirrors that provide several advantages. In theory, TIR provides a perfect (R=1) mirror, although in practice the reflectivity is less than unity due to surface roughness scattering and nonspecular transmission. However, ultra-smooth surfaces with root-mean-square surface roughness of ~0.05 nm can be generated routinely, providing equivalent mirror reflectivities of $R$~0.999999 in the visible region. The evanescent wave generated by TIR permits attenuated total reflectance (ATR)-like absorption measurements of condensed matter with EW-CRDS, but with much higher sensitivity. Several resonator designs for EW-CRDS have been developed. Initially, a prototype that incorporated a Pellin-Broca prism in a conventional CRDS cavity was demonstrated [7]. More recently, TIR-ring and monolithic folded cavity designs have been realized [10,11]. In the following, we limit our discussion to the TIR-ring and folded cavity, since these designs have the lowest intrinsic optical loss, have high-finesse for both polarization states, and are inherently miniature. The TIR-ring and folded cavity designs are first briefly reviewed. Application to water detection is then explored by evaluating the minimum intrinsic cavity losses and relative decay time uncertainties achievable with currently available technology.

## 2. OPTICAL RESONATOR DESIGNS

### 2.1 Total-internal-reflection-ring resonator

In addition to providing a convenient, low-loss sampling scheme for condensed matter, the use of TIR mirrors in EW-CRDS circumvents the narrow bandwidth associated with high reflectivity optical coatings. To fully utilize the broad bandwidth provided by TIR, an all-TIR cavity is required. The spectral bandwidth is then limited only by the transmission properties of the cavity medium. One general class of resonators that satisfy this requirement is the polygonal TIR-ring resonators [6,8,10,12], which support astigmatic, Gaussian modes that are well-described by products of Hermite-Gauss functions corresponding to the tangential and sagittal planes. In general, the angle of incidence at a TIR surface is given by $\theta_i=\pi(N\text{-}2)/2N$ for a ring resonator with $N$ facets, where a judicious choice is made for $N$ such that $\theta_i > \theta_c = \sin^{-1}(n_o/n_i)$ is maintained, given the ambient and cavity medium refractive indices, $n_0$ and $n_i$, respectively. Surfaces, films, or liquids can be probed with the polygonal TIR-ring resonator by selecting an appropriate resonator geometry in accord with the TIR condition. Furthermore, since TIR occurs for both the in-plane ($p$-) and out-of-plane ($s$-) polarization states, polarization-dependent phenomena such as

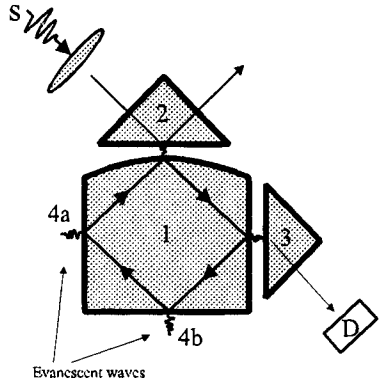


**Figure 1.** A miniature (<1 cm$^3$) polygonal, monolithic TIR-ring cavity (1) forms a novel cavity ring-down miniature spectrometer for condensed matter. Elements 2 and 3 are used to couple light into and out of the solid cavity by photon tunneling. Evanescent waves at positions 4a-b probe the surrounding medium. Measurement of the decay rate of an injected light pulse permits determination of the evanescent waves absorption. Input and output light beams can be transported by fiber-optics to remotely locate the light source (S) and detector (D).

molecular orientation can also be studied. As an example, a nominally square, monolithic TIR-ring cavity is depicted in Figure 1, which is the optimal fused-silica resonator used for spectroscopy of adsorbates or thin films in the visible or near infrared regions, given the refractive index range of $1.46 \geq n_i \geq 1.44$ over this spectral region. The square design is optimal since for $N$=4 the angle of incidence is closest to the critical angle, which maximizes the surface electric field enhancement [13]. Note that one facet of the resonator is convex with a radius of curvature that must satisfy separate stability criteria for the tangential and sagittal planes. A general derivation of the stability conditions and

lowest-order mode properties for polygonal TIR-ring resonators based on the round-trip transfer matrix can be found elsewhere[9].

Excitation and monitoring of cavity modes of a TIR-ring resonator is accomplished by photon tunneling. By approximating the astigmatic Gaussian modes of the resonator as a plane wave, Schiller *et al.*[12] derived an expression for the gap-width-dependent finesse for a square TIR-ring resonator, given by

$$\mathcal{F}(x)=\frac{\pi}{\beta(1+\exp(-2b(x-x_m)))} \tag{2}$$

with

$$b=\frac{2\pi}{\lambda_0}\sqrt{n_i^2\sin^2\theta_i-n_o^2} \tag{3}$$

where $\beta$ is the round-trip *field* attenuation, $x$ is the gap width variable, and $x_m$ is the impedance-matched gap width. For cavity ring-down measurements, the gap-width-dependent finesse has beneficial properties. In Figure 2

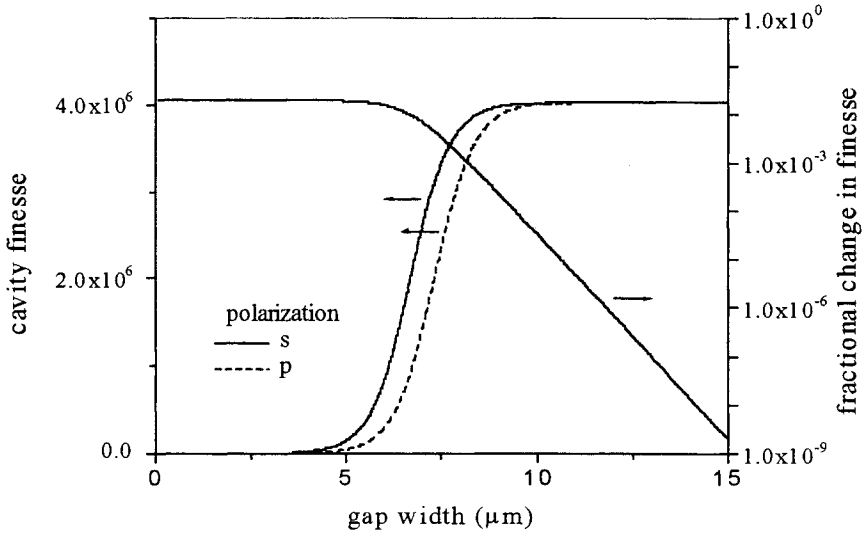


**Figure 2.** Cavity finesse is shown as a function of the gap width used for coupling light in and out of a square TIR-ring cavity by photon tunneling. The calculations for *s*-(solid) and *p*-(dashed) polarizations were obtained by assuming a plane wave to be incident on the tunneling junction. The point of inflection corresponds to the impedance-matched condition, where the on-resonance transmission is near unity. Also shown is the fractional change in finesse based on a 10-nm change in the gap width. By operating on the plateau at larger gap widths (>~9 um) the finesse is maximized and stabilized with respect to thermal and mechanical fluctuations, as indicated by the small and rapidly decreasing fractional change in finesse (right axis).

the calculated finesse is shown as a function of gap width in micrometers for *s*- and *p*-polarizations assuming a square, fused-silica resonator and 1380 nm excitation. The finesse is seen to increase with increasing gap width as the coupling loss decreases. At the point of inflection the impedance-matched condition is reached, where the coupling loss is equal to the sum of other round-trip losses. Beyond the impedance-matched gap width, the finesse approaches its maximum, uncoupled value. In this limit, the finesse and therefore the ring-down time is stabilized with respect to thermal or

mechanical fluctuations of the gap width, which should facilitate the development of a rugged, mobile sensor. Note also that the magnitude of the gap width in the weakly coupled limit is large, which leads to manageable fabrication and positioning tolerances.

## 2.2 Folded monolithic resonator

In chemical sensing applications where a single wavelength can be monitored to detect the analyte with certainty, the broad bandwidth of the TIR-ring resonator is not needed. Instead a monolithic folded resonator, as shown in Figure 3, can be used which employs both ultra-high reflective coatings and TIR [11]. Although the use of high reflectivity coatings restricts bandwidth, the folded resonator can be directly excited by a propagating wave thereby eliminating the complications associated with manipulating coupling optics for photon tunneling. The folded resonator also provides high finesse for both polarization states, excellent stability, and facile interfacing to a sample chamber.

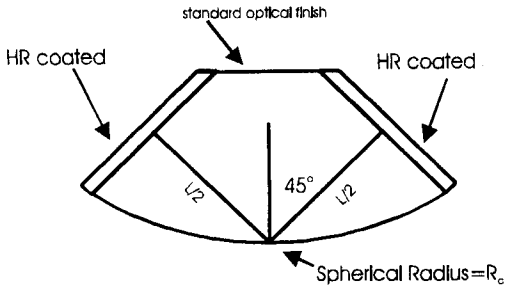


**Figure 3.** A monolithic, folded resonator for EW-CRDS is shown. The two high-reflectivity (HR), coated surfaces and the convex TIR surface form a stable optical cavity. Light is injected into the cavity through one of the coated surfaces to excite a cavity mode. The exponentially decaying intensity of the mode is detected as weak transmission through the second coated surface as in conventional CRDS. The flat surface that is opposite the convex surface facilitates mounting as well as interferometry for probing the thickness of films on the convex TIR surface. The evanescent wave, which emanates from the TIR surface, probes the sample absorption.

The three-mirror, folded resonator incorporates two planar ultra-high reflectivity coated surfaces and one convex TIR surface. Light is injected into the cavity through a planar coated surface to excite one or more cavity modes. The stability criteria for the sagittal and tangential planes have been derived elsewhere from the round-trip transfer matrix[9]. The absorption of an ambient medium is probed by the evanescent wave which emanates from the convex TIR surface. Surfaces, films, and liquids can be studied using the folded cavity by varying the design angle of incidence to maintain the TIR condition. In Figure 3, $\theta_i = 45°$ which is optimal for diagnostics of surfaces and films in the visible and near-IR using a fused silica resonator. Since TIR occurs for s- and p-polarizations states (though with different phase shifts) the folded cavity operates with high finesse for both polarizations, since the coated surfaces when employed at normal incidence do not result in significant depolarization. Hence a wide variety of polarization-dependent phenomena can be probed. Since the monolithic design of the resonator imparts stability to the mode frequencies, this design offers substantial potential for improved ring-down time measurement precision and therefore extremely high sensitivity.[14]

# 3. SIGNAL-TO-NOISE ANALYSIS FOR WATER DETECTION BY EW-CRDS

## 3.1 Resonator intrinsic loss

### 3.1.1 TIR-ring cavity

The sources of optical loss that arise for TIR-ring cavities have been investigated previously at 633 nm [6]. Here we examine the region around 1380 nm, where water has a combination band with a peak absorption cross-section of ~$10^{-18}$ $cm^2$/molecule. The objective is to predict the lowest possible detection limit for water based on currently available technology. In general, the total intrinsic optical loss for a TIR-ring resonator is well-approximated by the sum of the optical losses, which is given by

$$\mathcal{L}_0(\omega) = \mathcal{L}_{bulk} + \mathcal{L}_{diff} + \mathcal{L}_{nspec} + \mathcal{L}_{surf} + \mathcal{L}_{coup} \qquad (4)$$

where the terms correspond to cavity medium attenuation, diffraction losses, nonspecular transmission, TIR surface scattering, and coupling losses, respectively. It is important to note that Eqn. 4 neglects the contribution to the total loss arising from surface-bound species such as OH which are present on the nascent superpolished $SiO_2$ surface. Each loss term can be accounted for quantitatively by using an appropriate model. In the following, the cavity medium is assumed to be fused silica, which provides extremely high transmission in the region of interest for selected grades, having been thoroughly characterized for telecommunication purposes. Assuming a residual OH content of 50 parts-

per-billion (ppb) and an attenuation of 60 dB/km per 1000 ppb of OH, a bulk absorption coefficient for selected fused silica of $\alpha$ = 6.9 parts-per-million (ppm)/cm is possible at 1380 nm [15]. In the previous investigation at 633 nm, the opposing dependence on cavity size of bulk and diffraction losses was shown to give rise to an optimum size where the intrinsic loss minimizes for a given radius of curvature of the convex facet. Hence, when the TIR facet dimensions begin to approach the lowest order resonator mode dimensions, diffraction losses rise exponentially and are mode-dependent, while bulk attenuation decreases linearly according to $\mathcal{L}_{bulk}=\alpha \cdot L_{rt}$, where $L_{rt}$ is the round-trip path length. However, while nonspecular transmission was negligible in the previous analysis, in the near infrared we find that nonspecular losses greatly exceed diffraction losses. Nonspecular effects arise from the distribution of incident wave vectors associated with the finite (but unapertured) beam diameter [16]. A transmission loss results since a fraction of the incident distribution does not satisfy the TIR condition. The nonspecular loss is further enhanced by the decreasing index of refraction of fused silica with increasing wavelength. Using a simple model developed by Schiller [17], an upper bound for the nonspecular transmission of a Gaussian beam can be obtained which is given by,

$$\mathcal{L}_{nspec}(\xi)=\frac{1}{2}erfc(-\xi) \qquad (5)$$

where $\xi=(2\pi/\lambda_0)\,\omega_x(z)\,\sin(\theta_c-\theta_i)/\sqrt{2}$, $\lambda_0$ is the vacuum wavelength, $\omega_x(z)$ is the local beam radius in the tangential plane, and it is assumed that $R$=0 for $\theta_i < \theta_c$. Although $\mathcal{L}_{nspec} >> \mathcal{L}_{diff}$ was found for the conditions of interest, diffraction losses are incorporated in the following analysis. An estimate of $\mathcal{L}_{diff}$ is obtained by calculating the power loss arising from propagation of the fundamental (astigmatic) resonator mode through an aperture with tangential dimension, $x_a$, which is obtained by projection of the cavity facet dimension in the beam direction. The diffraction loss is then approximated by,

$$\mathcal{L}_{diff}=-\ln\left(erf\left(\frac{x_a}{\sqrt{2}\omega_x(z)}\right)\right) \qquad (6)$$

where again $\omega_x(z)$ is the tangential beam radius at the relevant facet, which has been propagated from the cavity waist. Only the tangential plane is considered since this dimension is linked to other losses through $L_{rt}$, while the sagittal dimension can be chosen arbitrarily. Eqn. 6 is valid when the aperture dimension is large relative to the mode size [18], defined by the $1/e^2$ diameter. The remaining losses in Eqn. 4, $\mathcal{L}_{surf}$ and $\mathcal{L}_{coup}$, are modeled by approximating the Gaussian resonator mode as a plane wave. Surface scattering losses are estimated from the surface RMS surface roughness, $\sigma$, according to

$$\mathcal{L}_{surf}=N\left(\frac{4\pi n_i \sigma \cos\theta_i}{\lambda_0}\right)^2 \qquad (7)$$

where $n_i$ =1.446 for fused silica at 1380 nm. It is worth noting that the surface RMS roughness, which can be measured by precision interferometry or profilometry, does not necessarily correlate with the military scratch-dig specification which is commonly provided by optics manufacturers. The remaining loss term, $\mathcal{L}_{coup}$, can be calculated for the TIR-ring cavity by using the expression derived by Court and von Willisen [19] for transmission with 'frustrated total internal reflection', given by

$$\mathcal{L}_{coup}(x)=\frac{1}{\psi(n_i,n_0,\theta_i)\sinh^2 K(n_i,n_0,\theta_i)x+\chi(n_i,n_0,\theta_i)} \qquad (8)$$

where the parameters $\psi$, $K$, and $\chi$ are function of the angle of incidence and refractive indices as indicated. Eqn. 8 describes photon tunneling through a single junction when an optically dense, semi-infinite medium (the coupling optic) is brought within the decay length of the evanescent wave. However, as noted previously, in order to operate in the weakly coupled regime that stabilizes finesse with respect to fluctuations in the cavity-coupler separation, the coupling loss is adjusted to be a small fraction (~0.005, *vide infra*) of the remaining intrinsic cavity loss. Therefore, to estimate the optimal sensitivity for water detection, the minimum intrinsic loss is first found, excluding coupling. The coupling loss is then determined by a judicious selection of cavity-coupler separation, based on stability requirements. This choice of cavity-coupler separation then establishes the on-resonance transmission of the ring-down cavity. With knowledge of the input beam characteristics, the output signal level can be determined, which enters into the evaluation of the ring-down time measurement precision. The best achievable sensitivity is then the product of the minimum achievable loss and the best achievable relative decay time precision.

Plots of Eqn. 4, excluding the coupling loss, are shown in Figure 4 as a function of $L_{rt}$, for $R_c/L_{rt}$=1,5,10, 100 where $R_c$ is the radius of curvature of the convex facet. Each value of $R_c/L_{rt}$ specifies a particular cavity design so that the same cavity is re-scaled to a different inscribed circle diameter $d_0=L_{rt}/N\sin(\pi/N)=\sqrt{2}L_{rt}/4$

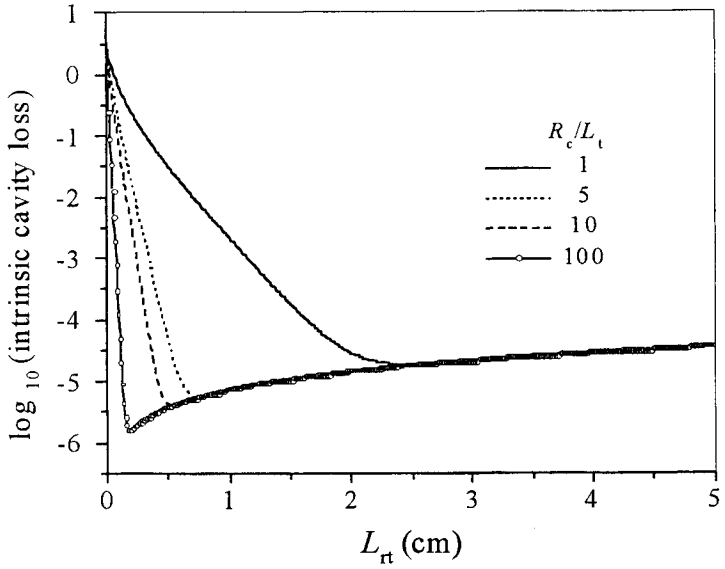


**Figure 4.** The intrinsic loss for four cavity designs with $R_c/L_{rt}$= 1(solid), 5(dotted), 10(dashed), and 100 (line with open circles) is plotted as a function of the round-trip path length, $L_{rt}$. A minimum intrinsic loss is found for each design that becomes more pronounced as $R_c/L_{rt}$ increases. The minimum loss is used to calculate the lowest achievable detection limit for water at 1380 nm. Note that increasing $R_c/L_{rt}$ reduces the minimum loss, but will ultimately increase the diffraction contribution to the total loss as the resonator approaches the unstable limit in which all facets are flat.

for each $L_{rt}$ in Figure 4. Note that a minimum loss is found for each design which shifts to smaller cavity sizes and deepens with increasing $R_c/L_{rt}$. The minimum loss of 1.56 ppm is obtained for $R_c/L_{rt}$=100 at $L_{rt}$=1.8 mm or $d_0$=636 um. A somewhat smaller minimum could be obtained for larger $R_c/L_{rt}$, since the nonspecular loss is reduced by increasing the mode waist size. However, diffraction losses eventually begin to dominate at significantly smaller cavity sizes. Figure 5 shows the contribution of nonspecular and diffraction losses to the total loss for the $R_c/L_{rt}$=100 case. The position and depth of the minimum is seen to be determined by the competition between nonspecular and bulk losses. Diffraction losses, which are described by the dashed line, contribute only for relatively small cavity sizes. Of course, in the limit $R_c/L_{rt}\rightarrow\infty$, the resonator becomes borderline unstable, so that diffraction losses will then dominate. Considering the case of $R_c/L_{rt}$=100 for the estimate of sensitivity, the calculated finesse, which is shown in Figure 2, reaches a constant value to within $\sim 1\times10^{-4}$ at a cavity-coupler separation of 9.4 μm, assuming fluctuations in the gap width of $\leq$10 nm are permissible.

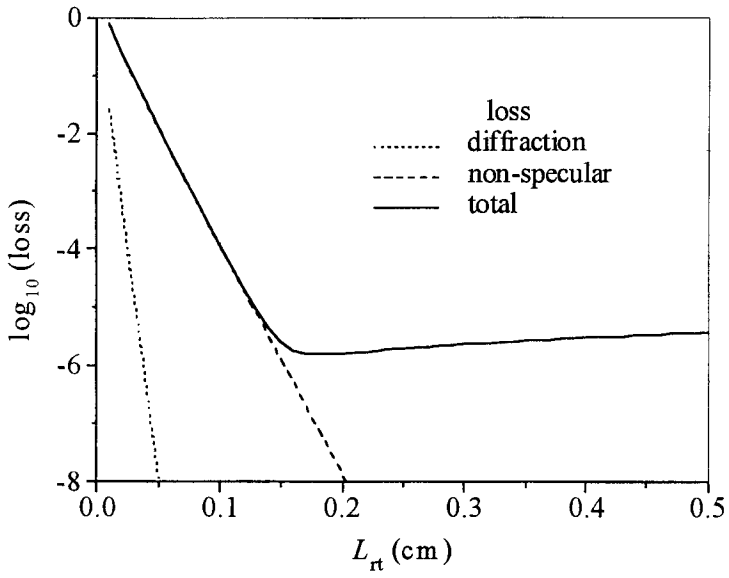


**Figure 5.** The total (solid line), nonspecular (dashed), and diffraction (dotted) losses are shown as a function of $L_{rt}$ for a TIR-ring cavity with $R_c/L_{rt}$=100. The minimum in the total loss arises from the nonspecular and bulk losses. Diffraction losses are less important at 1380 nm unless $R_c/L_{rt}$ is very large.

Figure 6 shows the calculated transmission [12] through a square TIR-ring cavity, with $\mathcal{L}_0(x) = 1.56\times10^{-6} + \mathcal{L}_{coup}(x)$ as a function of $x$, the cavity-coupler separation. At 9.4 μm, the cavity transmission is 2.0 % on resonance, which together with the cavity linewidth permits the output signal level to be estimated for a given input power and source linewidth.

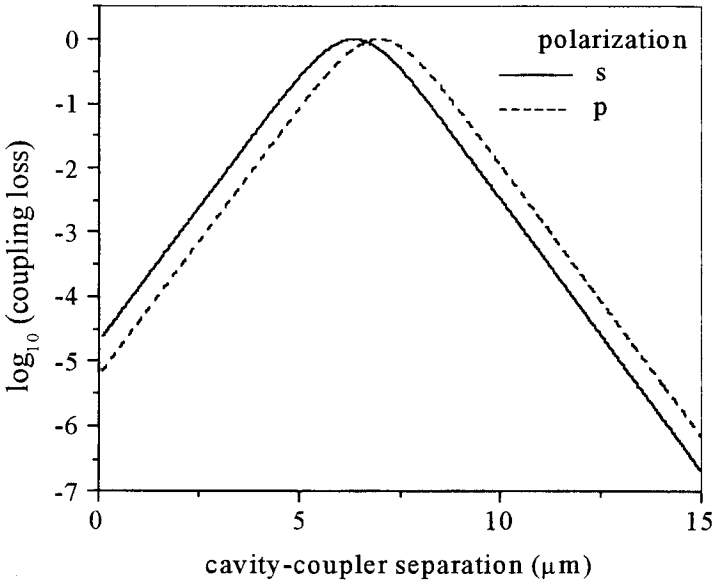


**Figure 6.** The logarithm of the cavity transmission is plotted as a function of the cavity-coupler separation, $x$, for a cavity with an intrinsic loss of $\mathcal{L}_0(x) = 1.56\times10^{-6} + \mathcal{L}_{coup}(x)$. At 9.4 μm, the cavity transmission is 2% which provides ample signal while stabilizing the finesse through operation in the weakly coupled plateau region of Figure 2.

### 3.1.2 Monolithic folded resonator

For the monolithic, folded resonator the analysis of optical losses is similar to the TIR-ring cavity, although the coupling loss is fixed by the transmission of the high reflectivity coated surfaces. In addition, the surface loss term,

$\mathcal{L}_{surf}$, can be decomposed into contributions from roughness-induced scattering by both the TIR and coated surfaces and an absorption loss due to the coating material.

### 3.2 Decay time measurement precision

A detailed analysis of decay time measurement precision in CRDS has been presented elsewhere[14]. As noted previously, the minimum detectable absorption in any CRDS measurement is proportional to the product of the intrinsic cavity loss and the relative uncertainty in the ring-down time measurement. In this section we evaluate the ring-down time measurement precision using realistic system parameters based on currently available technology for operation at 1380 nm. The impact of future advancements in technology will also be apparent. In general, the ring-down time is determined through a least-squares fit of the decay signals, yielding the value of the ring-down time, $\tau$, that minimizes the mean square deviation of the fit residuals. The observed signals are typically modeled by the expression

$$S(t) = S_0 \exp(-t/\tau) + S_{bl} + \varepsilon(t) \qquad (9)$$

where $S_0$ is the signal level at $t$=0, $S_{bl}$ is the baseline offset, and $\varepsilon(t)$ represents system noise. A single ring-down time measurement and fit yields a value for the standard deviation, $\sigma_\tau$, which is ultimately limited by photon shot noise. In practice, technical noise typically dominates, which arises from amplifier and detector noise, digitization errors, and non-exponential behavior of the decay signal. Precision is optimized by employing low noise amplifiers, high accuracy digitizers, and by exciting only a single cavity mode in a given measurement, which yields nearly pure exponential decays.

In the following, we assume single cavity mode excitation, which requires the incident excitation source to match a single cavity mode both in the longitudinal and transverse mode indices. Single longitudinal modes, the spacing of which is determined by the cavity free spectral range (FSR = $c/nL_r$), are individually excited when the source bandwidth is sufficiently less than the FSR and the source center frequency corresponds to a mode center frequency. This condition should be more easily achieved for EW-CRDS than standard CRDS, because the relatively small, monolithic resonators employed have a large FSR, which decreases excitation of adjacent modes. Single transverse modes are individually excited when the incident transverse profile is efficiently shaped to match the transverse profile of the cavity mode. We further assume in the following analysis that digitization errors can be neglected, indicating in the final analysis the limitation of this choice. Under these assumptions, the relative standard deviation derived from fitting a single ring-down decay signal is found to be

$$\sigma_\tau/\tau = \sqrt{\frac{h\nu}{\eta P_p \tau} + \frac{5\,NEP^2}{P_p^2 \tau}}\,, \qquad (10)$$

where $P_p$ is the peak power in the signal, $\eta$ is the quantum efficiency of the photodetector, $h\nu$ is the photon energy, and *NEP* is the *effective* noise equivalent power of the detection system. The first term in Eqn. 10 corresponds to shot-noise, while the second term corresponds to technical noise. This expression is valid for pulsed or cw excitation of the ring-down cavity under conditions of single-mode excitation. The *NEP* includes noise arising from the photodetector, amplifiers, cabling *etc.* Equation 10 is valid when the system statistics are described by the single-shot standard deviation. Often in practice, the single-decay-measurement standard deviation given by Eqn. 10 is smaller than the standard deviation of an ensemble of decay measurements. This indicates the presence of system variability occurring on time scales exceeding $\tau$, which is not explicitly accounted for in the above analysis. These sources of variability can be eliminated as demonstrated previously.[14] Assuming equivalence between the single-shot standard deviation given above and the standard deviation of an ensemble of measured ring-down times, the minimum detectable change in absorption is,

$$\Delta\mathcal{L}_{min} = \mathcal{L}_0 \sqrt{\frac{2}{n_s}} \frac{\sigma_\tau}{\langle\tau\rangle} \qquad (11)$$

where $\langle\tau\rangle$ is the ensemble average of the time constant determined by fitting $n_s$ measurements. In Figure 7, Eqn. 11 is plotted for $n_s$=100, illustrating the dependence of $\Delta\mathcal{L}_{min}$ on $P_p$ with system *NEP* as a parameter.

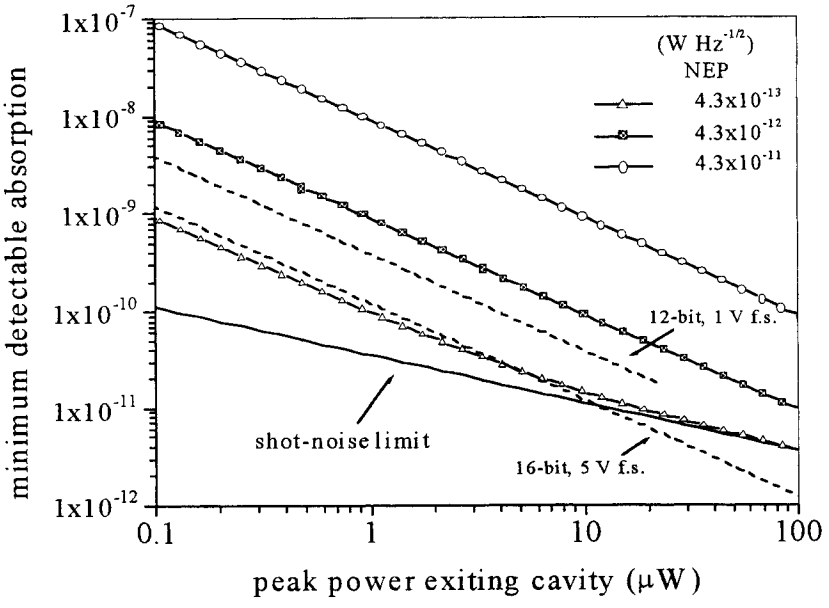


**Figure 7.** The minimum detectable absorption, $\Delta\mathcal{L}_{min}$, calculated according to Eqns.10-11 is shown for the square TIR-ring cavity with $L_{rt}$ = 1.8 mm and $\mathcal{L}_0$ = $1.57\times10^{-6}$. For all calculations, $\eta$ = 1 and $n_s$ = 100. The solid line corresponds to the shot-noise-limited case. The two dashed lines indicate the lower limits associated with the finite vertical resolution of 12- and 16-bit A/D data acquisition modules having the specified full-scale ranges of 1 V and 5 V, respectively. The signal levels at the digitizer are based on a photoreceiver responsivity of $4\times10^4$ V/W, and the required bandwidth for the system is ≈ 1 MHz. Assuming a coupler gap width of 9.4 μm, the minimum cw power incident on the resonator required is ≈50 $P_p$.

The choice of $n_s$ determines the system response time, which for $n_s$=100 would typically be 10 s or less. The calculations shown in Figure 7 are for a square, TIR-ring cavity with an intrinsic minimum loss of $1.57\times10^{-6}$ and $L_{rt}$ =1.8 mm as discussed above, which yields a ring-down time of $\tau$ = 5.54 μs and an effective cavity linewidth of 60.1 kHz. Three values of the *NEP* are selected. The intermediate value given by *NEP* = $4.3\times10^{-12}$ W $Hz^{-1/2}$ corresponds to the effective *NEP* of a low-noise photoreceiver (InGaAs detector and amplifier with a bandwidth of 125 MHz, quantum efficiency near unity in the spectral range 0.9 to 1.7 μm, responsivity of $4\times10^4$ V/W and *NEP*= $2.5\times10^{-12}$W $Hz^{-1/2}$ ) in series with the input amplifier of a 12-bit digitizing module (bandwidth of 50 MHz with an rms noise of 1 mV, and 1 V full-scale signal). Both of these systems are commercially available. The other two *NEP* values considered bracket the commercially available value by an order of magnitude in each direction. Also, shown in Fig. 7 is the shot-noise-limited case indicated by the heavy solid line. At fixed *NEP*, $\Delta\mathcal{L}_{min}$ decreases with increasing $P_p$ and approaches shot-noise-limited values for all cases. For the two largest *NEP* values, a 12-bit vertical resolution is adequate for all $P_p$ in the range 0.1 to 100 μW. For $P_p$ =15 μW and with a system *NEP* = $4.3\times10^{-12}$ W $Hz^{-1/2}$, $\sigma_\tau/\tau=2.8\times10^{-4}$ which corresponds to $\Delta\mathcal{L}_{min}= 6.1\times10^{-11}$. With 16-bits of vertical resolution and the selected *NEP* which is 1/10 of the commercially available *NEP* = $4.3\times10^{-12}$ W $Hz^{-1/2}$, the minimum detectable absorption is within 20% of the shot-noise limit for $P_p \geq 15$ μW. However, this combination of *NEP* and digitizer resolution begins to exceed the capability of commercially available technology, although we note that some improvement in *NEP* would be likely with a custom-designed system (photoreceiver and digitizing module) having the minimum required bandwidth of $5\tau^{-1} \approx$ 1 MHz.. Finally, we note that a coupler gap width of 9.4 μm (as discussed above) gives a system transmittance of ≈2% for excitation by a perfectly mode-matched and monochromatic cw laser source. Even with additional insertion losses

of 90% that could result from mode-matching a several hundred kHz linewidth source, such as an external cavity diode laser, into the high-finesse TIR-ring cavity (linewidth = 60 kHz), a $P_p$ of 15 μW (discussed above) could be achieved with an incident beam power of 10 mW - a fluence that is within the range of existing frequency-stabilized single-mode diode lasers.

## 4. CONCLUSION

Employing realistic estimates for optical and detection system parameters and assuming an average of 100 decay time measurements, which can be accomplished in ≤ 10 s, we have shown that a minimum detectable absorption of $6.1 \times 10^{-11}$ can be achieved with existing technology at 1380 nm, assuming an intrinsic cavity loss of $1.57 \times 10^{-6}$ and a relative decay time measurement precision of $2.8 \times 10^{-4}$. To estimate the minimum detectable gas phase water concentration that can be achieved with EW-CRDS, the absorption cross-section, molecular orientation, sticking coefficient, and saturation coverage of surface-bound water become influential. Many of these parameters have been addressed recently in studies in ultra-high vacuum with well-characterized $SiO_2$ surfaces by Sneh *et al.* [20] Indeed the initial sticking coefficient for a wide variety of practically accessible conditions of pressure and temperature was found to be unity. Furthermore, in related work the different forms of surface OH on a fully hydroxylated surface have been characterized in some detail, as well as conditions for removing the OH layer.[21] It is important to note that in practice, the minimum intrinsic cavity loss may be strongly influenced by nascent surface-absorbing species such as surface-bound OH. This has the adverse effect of increasing the intrinsic loss of the cavity. Yet the OH groups also act effectively as a molecular-recognition film for water through hydrogen-bonding interactions. Future studies will be needed to resolve these key issues, which become critical in the development of a water sensor and provide insight into the interactions of water with the technologically important $SiO_2$ surface. It is also interesting to speculate that at the highest sensitivity levels discussed above, density fluctuations, which are precursory to single-molecule detection, would become measurable.

## ACKNOWLEDGMENTS

The authors gratefully acknowledge support through the Environmental Management Science Program (EMSP) of the Department of Energy under Contract DE-AI07-97ER62518.

## REFERENCES

1. A. O'Keefe and D. A. G. Deacon, Rev. Sci. Instrum. **59**, 2544 (1988).
2. J. J. Scherer, J. B. Paul, A. O'Keefe, R. J. Saykally, *Chem. Rev.* **97**, 25, (1997).
3. M. D. Wheeler, S. M. Newman, A. J. Orr-Ewing, M. N. R. Ashfold, J. Chem. Soc. Faraday T. **94** (3), 337, (1998).
4. *Cavity-Ringdown Spectroscopy*, K. W. Busch and M. A. Busch, eds. (Oxford University Press, 1999).
5. P. Zalicki and R. N. Zare, J. Chem. Phys. **102**, 2708, (1995).
6. A. C. R. Pipino, J. W. Hudgens, R. E. Huie, Rev. Sci. Instrum. **68** (8), 2978, (1997).
7. A. C. R. Pipino, J. W. Hudgens, R. E. Huie, Chem. Phys. Lett. **280**, 104 (1997).
8. A. C. R. Pipino in advanced Sensors and Monitirs for Process Industries and the Environment, Wim A. De Groot, editor, Proc. of SPIE, Vol. 3535, p 57, Boston, Mass. 1998.
9. A. C. R. Pipino in Advanced Materials and Optical Systems for Chemical and Biological detection, M. Fallahi and B. I. Swanson, Eds., Proc. SPIE Vol. 3858, p74, Boston, Mass. (1999).
10. A. C. R. Pipino, Phys. Rev. Lett. **83**(15), 3093,(1999).
11. A. C. R. Pipino, Appl. Opt. **39** (9), 1449, (2000).
12. S. Schiller, I. I. Yu, M. M. Fejer, and R. L. Byer, Opt. Lett. **17**, 378 (1992).
13. N. J. Harrick, *Internal Reflection Spectroscopy*, (Interscience Publishers, New York, 1967).
14. R. D. van Zee, J. T. Hodges, and J. P. Looney, Appl. Opt. **38**, 3951 (1999).
15. Private communicate, Grant Lu, Amersil Corp.

16. J. J. Regan and D. R. Andersen, Comput. Phys. **49**, 49, (1991).
17. S. Sciller, Ph. D. Thesis, Stanford University, 1993.
18. K. Ait-Ameur, H. Ladjouze, and G. Stephan, Appl. Opt. **31** (3), 397, (1992).
19. I. N. Court and F. K. Von Willisen, Appl. Opt. **3**, 719, (1964).
20. O.Sneh, M.A. Cameron, S.M. George, Surf. Sci., **364**, 61, (1996).

21. O.Sneh, M.A. and S.M. George, J. Phys. Chem., **99**, 4639, (1995).

## Disclaimer

Identification of specific commercial products in this paper is provided in order to specify procedures completely. In no case does such identification imply recommendation or endorsement by the National Institute of Standards and Technology, nor does it imply that such products have necessarily been identified as the best available for the purpose.